Journal of Sound and Vibration 329 (2010) 2349–2366

Contents lists available at ScienceDirect

Journal of Sound and Vibration

journal homepage: www.elsevier.com/locate/jsvi

The use of pseudo-faults for novelty detection in SHM

Evangelos Papatheou, Graeme Manson, Robert J. Barthorpe, Keith Worden *

Dynamics Research Group, Department of Mechanical Engineering, University of Sheffield, Mappin Street, Sheffield S1 3JD, UK

ARTICLE INFO

Article history:
Accepted 22 July 2009
The peer review of this article was organised by the Guest Editor
Available online 18 August 2009

ABSTRACT

The main problem associated with pattern recognition based approaches to Structural Health Monitoring (SHM) is that damage localisation and quantification almost always require supervised learning. In the case of high-value engineering structures like aircraft, it is simply not possible to generate the training data associated with damage by experiment. It is also unlikely that data can always be generated by simulation as the models required would often need to be of such high fidelity that the costs of development and the run-times would again be prohibitive. The object of this paper is to explore the potential of a simple experimental strategy, which involves adding masses to the structure, in the attempt to extract features for novelty detection. The idea itself is not presented as revolutionary based on the fact that adding masses has been considered as a case of damage before, however, an in-depth investigation of its suitability for guiding feature selection is presented here. The approach is illustrated first on a simple structure by using data generated from a finite-element (FE) simulation and then validated experimentally on a more complicated laboratory structure. Simulated damage, in the form of a loss in the stiffness in the case of the numerical model and of a saw-cut in the case of the structure is used for comparison. The results show similar patterns in both cases which suggests a potential use of the method for higher level damage detection.

1. Introduction

A structure is generally called *damaged* when it no longer operates in its designed and ideal condition, but it can still function in a sub-optimal but satisfactory way. If this *damage* is left to develop it will eventually affect the system's performance in such a way that it no longer meets its design standards set by engineers and therefore is unacceptable. This situation can be defined as a *fault* and should be avoided for the danger to life and the high costs it conveys. The earliest possible detection of this state could easily bring many economic benefits to various industries.

There are a large number of non-destructive evaluation (NDE) methods currently available for the local inspection of structures [1]. Although highly effective and sensitive, these methods usually require *a priori* knowledge of the area of interest and have a substantial cost. In addition, they demand a large degree of expertise, can be time consuming and in general work only in accessible areas of the structure. It is against this backdrop that the highly active research field of Structural Health Monitoring (SHM) arises with the ultimate purpose of developing a robust, reliable and global monitoring method. In general, the SHM approaches to identifying damage have concentrated upon changes to the dynamic properties of the system. Doebling et al. [2] have published an extensive literature review of such vibration-based methods.

* Corresponding author.
E-mail addresses: mep05ep@sheffield.ac.uk (E. Papatheou), g.manson@sheffield.ac.uk (G. Manson), r.j.barthorpe@sheffield.ac.uk (R.J. Barthorpe), k.worden@sheffield.ac.uk (K. Worden).

0022-460X/$ - see front matter © 2009 Elsevier Ltd. All rights reserved.
doi:10.1016/j.jsv.2009.07.020

Overall, the problem of damage detection can be considered to have a certain hierarchical structure with questions posed at different levels. Perhaps the most well-known such framework is that of Rytter [3] with four levels of damage identification; namely, Level 1—detection, Level 2—localisation, Level 3—assessment and Level 4—prognosis. It is reasonable to say that the higher one goes up the scale the harder the problem becomes. There have been many methods proposed to address the first level and some of them have been quite successful; this is not generally the case for the other levels. Pattern recognition (PR) is a data-driven approach to damage identification that can be used for higher detection levels. However, an attempt to progress up the levels will almost certainly make the use of supervised learning a necessity, which inevitably requires the existence of training data from all possible damage states. It may be feasible to acquire such data when dealing with relatively simple and low-cost structures, but it will become a serious obstacle in experiments involving high-value structures such as aircraft.

One way to cope with this situation is to generate data by simulation, but in order to obtain realistic results, validated models of high fidelity are required. Such models are going to be significantly time-consuming when running, as well as very expensive to develop. That is why the question of how to extract damage-sensitive features without actually damaging the structure becomes imperative. In the current paper the very simple approach of adding masses to a system in order to support feature selection is explored. The idea is based on the knowledge that damage will introduce a local flexibility to the system. If the simple formula for a SDOF system $\omega = \sqrt{k/m}$ is blithely extrapolated, then it might appear reasonable to assume that the change in natural frequency caused by a stiffness loss could also be caused by an increase in the structure's mass.

Adding masses as a form of damage simulation, among others, has been used before, as in [4–6], and exclusively added mass localisation has been tried in [7,8]. However, the exact idea of actually comparing added mass with stiffness loss to guide feature selection has only been attempted previously in [9], and this study itself involved only preliminary tests. A much more comprehensive study is made here, FE analysis is used to model a cantilever aluminium beam and to generate its frequency response function or FRF. Then, damage is introduced as a reduction in the Young's modulus and later as an increase in the beam's density. The two scenarios are compared accordingly and novelty detectors are created. The approach is next extended to a laboratory structure-a plate incorporating stiffening elements-designed to model an aircraft wingbox.

The layout of the paper is as follows. The next two sections describe the numerical simulation; the first is involved with the FE model of the beam, followed by results and the second discusses the construction of novelty detectors from it. The last two sections of the paper are involved with the experimental part of the work; the first of these describes the test setup and discusses the data acquisition and the second considers the feature selection and the novelty detection on the wingbox structure. Finally, the paper is rounded off with some conclusions and a discussion of the actual potential of the approach.

2. Numerical simulation

The role of numerical simulation in the development of SHM methodologies is a little problematical. It is certainly true to say that the final arbiter in all cases should be experiment; however, it would be unwise to completely disregard the advantages that simulation offers. That said, it must be acknowledged that SHM algorithm development can no longer be justified on the basis of highly simplified models; the days when an algorithm is considered to be validated *solely* on the basis of results from a simulated cantilever beam have come and gone. In this spirit, the numerical simulation presented here is not offered in sole support of the proposed methodology; however, the authors have included it in the belief that it does prove to be an interesting first step in the direction of validation.

2.1. FE model of the beam

The beam considered here has dimensions of 750 mm in length and its cross-section is 10 mm × 30 mm. The material properties for aluminium are taken as: Young's modulus $E = 70$ GPa, Poisson's ratio $\nu = 0.3$ and density $\rho = 2710\,\mathrm{kg\,m^{-3}}$. The FE analysis package MATFEM [10] was used for all modelling and calculations at this stage. The elements used were beam elements; to be specific, 2-noded uniaxial elements where each node has 6 degrees of freedom. They are based on Timoshenko's well-known theory of vibration, taking into account shear and torsion. In total 30 elements were used, which means that each one had a length of 2.5 cm.

A cantilever beam is rather a simple model to require the use of a FE package; however, FE analysis was employed here because it offered the possibility of generating more advanced features like FRFs and transmissibilities. In order to verify the model itself, the natural frequencies found by FE modal analysis were compared with those calculated from formulae in Blevins [11]. Since there was very close agreement in the lower bending modes (up to the 10th) and the first three torsion modes, the overall beam model was judged as good enough for the study.

2.2. Results from the numerical FE model

As stated before, the aim of this paper was to explore the possibility of adding masses to a system in order to extract damage-sensitive features and to define an experimental strategy for achieving this. A very simple and well-known

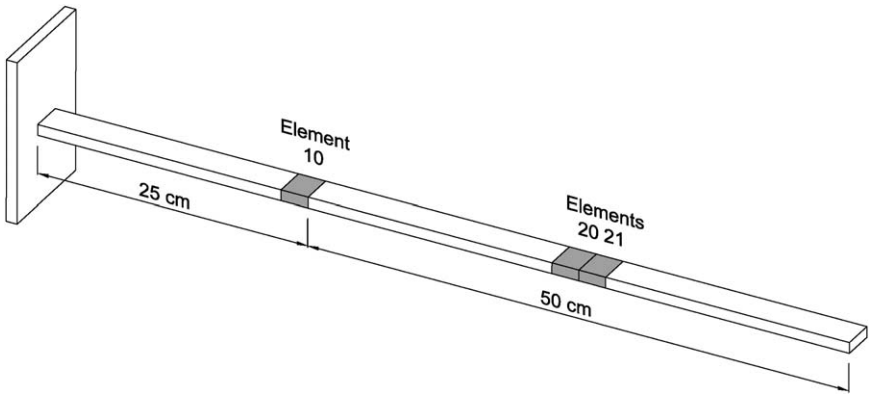

Fig. 1. Location of the three elements to which damage was introduced during the first part of the study (FE simulation).

Table 1
The effect of stiffness reduction and density increase on the first 10 bending modes of the beam.

Healthy	$E = 46.67$ GPa (Hz)	$\rho = 4065\,\mathrm{kg\,m^{-3}}$
14.596	14.585	14.441
91.452	90.510	91.039
255.970	251.476	252.486
501.317	499.656	499.941
828.118	824.490	824.237
1235.996	1217.664	1217.517
1724.584	1716.051	1715.938
2293.478	2286.790	2286.563
2942.253	2902.329	2902.769
3670.490	3645.694	3645.671

indication that a system or structure is damaged is that its natural frequencies change, and in most cases drop; this was the first approach considered here also. Damage was initially introduced to the 21st element (see Fig. 1) of the model (50 cm from the clamped end) as a reduction in the Young's modulus from 70 to 46.67 GPa (2/3rds of the initial value) and later as an increase of the density from 2710 to 4065 kg m^{-3} (3/2nds of the healthy value). The first 10 bending modes of the beam were then compared and can be seen in Table 1; as anticipated, in both cases, they are lower than the healthy state.

A *feature* is basically some set of values derived or calculated from measured data. Here, the features considered were frequency and magnitude values from FRF resonance peaks and from transmissibility functions. All data used at this stage were provided by simulation. So, with the aid of the FE package MATFEM, FRFs of the beam at various locations were calculated. Since the input is always the same, it is straightforward to derive a transmissibility function defined as the ratio of two FRFs: $T(\omega) = H_1(\omega)/H_2(\omega)$. An example of an FRF function of the beam under flexural excitation at its free end can be seen in Fig. 2.

As it was shown that adding masses to the beam lowers its frequencies, the next step was a more thorough investigation. It was decided that, in order to make the approach more subtle, three damage levels of each case would be applied in two separate locations along the beam. Those locations were at the element 10 (22.5 cm from the clamped end) and element 20 (47.5 cm from the clamped end) as seen in Fig. 1. Stiffness reductions were sequentially made from 70 to 60, 50 and 40 GPa. The element density was separately increased to a value equivalent to an added mass of 10, 20 and 30 g, which corresponds to 1.64, 3.28 and 4.92 percent of total mass increase.

By using MATFEM, the driving-point FRF at the free end of the beam was calculated. Next, the 4th, 6th and 7th bending modes (selected as being typical of the set) from the magnitude of each FRF for each case were compared. Figs. 3 and 4 show the effect of damage (stiffness reduction and density increase) on the 4th mode of the beam in two separate locations (elements 10 and 20). Results from all the three modes (4th, 6th and 7th) are summarised in Tables 2 and 3, where the frequency and magnitude shift (in percentage form and relative to dB) for each FRF peak from the healthy state is displayed for different levels of damage.

As expected, the natural frequencies of the beam (approximated by the FRF peaks) become smaller with the introduction of more severe damage. With the symbol '–' it is stated that the peaks move to lower dB levels or Hz values, otherwise they move to higher. An important point here is that the FRFs were calculated with a uniform resolution of 0.5 Hz. This is the main reason why in Fig. 4 and in Table 3 there seems to be a zero frequency shift on the 4th mode, since the actual difference (found by FE modal analysis) is smaller than the value of 0.5.

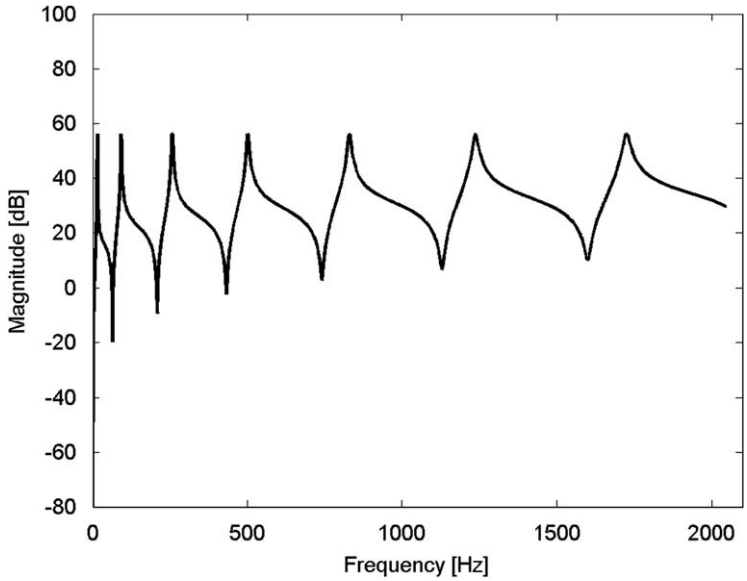

Fig. 2. FRF calculated by MATFEM when the excitation and the response were at the free end of the beam (normal state).

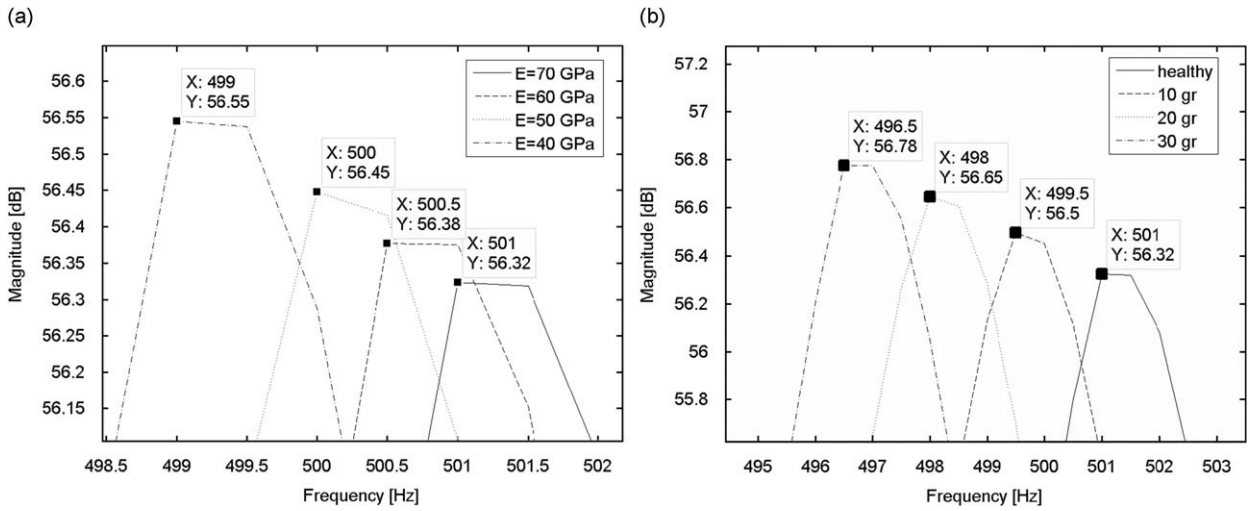

Fig. 3. The effect of stiffness reduction (a) and density increase (b) on the 4th mode of the beam. The fault was introduced in element 10 (FRF as in Fig. 2).

It is clear that damage in different locations does not affect the modes in the same way-something expected and already known-but it seems quite promising that the results of the stiffness reduction and density increase show similar patterns. This can be clearly seen in Figs. 3 and 4: the peaks (4th mode) move to higher dB levels when the fault is introduced in element 10 for both stiffness reduction and density increase, but then they move to lower levels when the fault is introduced in element 20. This behaviour can be clearly seen in Tables 2 and 3, and to be specific, in the magnitude shift columns.

3. Construction of novelty detectors from the numerical model

In order to construct novelty detectors, there was the need for feature extraction. As stated previously, transmissibility functions were calculated by taking the ratio of two FRFs. The first step was to follow the same procedure as before for the three modes of the response FRF (4th, 6th and 7th), but this time on the transmissibility peaks and troughs. Of course in a transmissibility function, the peaks are not usually at the same frequencies as the modes of the structure, but are expected to be sensitive to damage. Fig. 5 shows the transmissibility used in this stage, formed from two response FRFs, one at 75 cm over the one at 25 cm when the excitation was at the free end of the beam (75 cm).

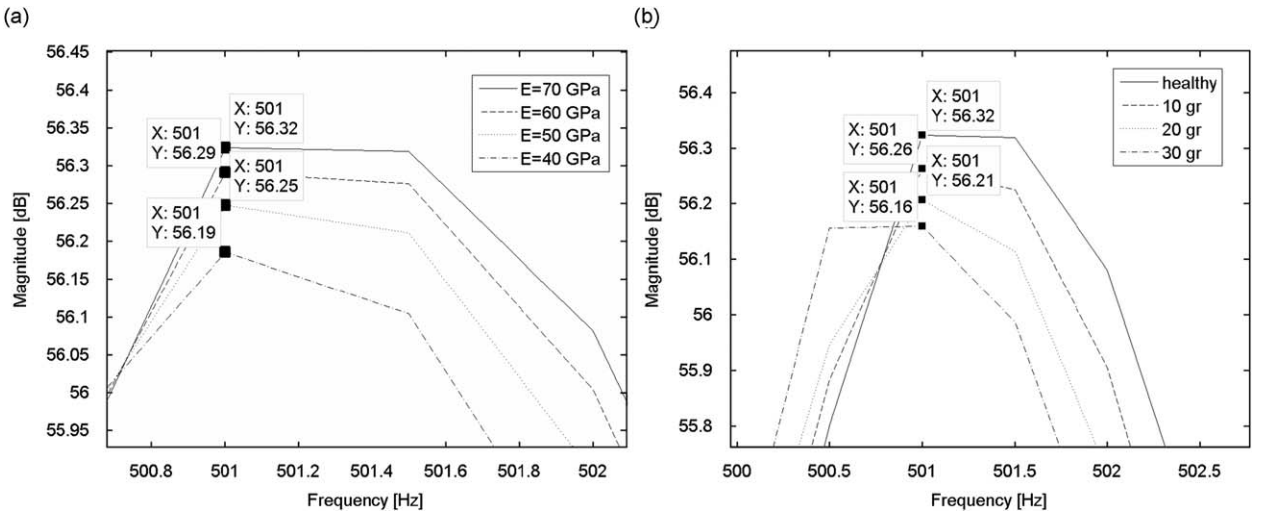

Fig. 4. The effect of stiffness reduction (a) and density increase (b) on the 4th mode of the beam. The fault was introduced in element 20 (FRF as in Fig. 2).

Table 2
Effect of stiffness reduction and density increase in element 10 on the 4th, 6th and 7th mode of the beam.

Mode no.	Stiffness reduction			Density increase		
	E (GPa)	Frequency shift (Percent)	Magnitude shift (Percent)	Added mass (g)	Frequency shift (Percent)	Magnitude shift (Percent)
4	60	−0.01	0.09	10	−0.01	0.31
	50	−0.20	0.22	20	−0.60	0.57
	40	−0.40	0.39	30	−0.90	0.80
6	60	−0.57	−0.05	10	−1.45	−0.10
	50	−1.29	−0.09	20	−2.75	−0.13
	40	−2.18	−0.11	30	−3.80	−0.13
7	60	−0.17	0.21	10	−0.46	0.56
	50	−0.41	0.48	20	−0.87	0.99
	40	−0.70	0.82	30	−1.22	1.33

The frequency and magnitude shift (relative to dB) in percent from each peak (fault severity) to the healthy is shown.

Table 3
Effect of stiffness reduction and density increase in element 20 on the 4th, 6th and 7th mode of the beam.

Mode no.	Stiffness reduction			Density increase		
	E (GPa)	Frequency shift (Percent)	Magnitude shift (Percent)	Added mass (g)	Frequency shift (Percent)	Magnitude shift (Percent)
4	60	0	−0.06	10	0	−0.11
	50	0	−0.13	20	0	−0.21
	40	0	−0.24	30	0	−0.29
6	60	−0.40	−0.42	10	−1.13	−1.21
	50	−0.89	−0.98	20	−1.94	−2.30
	40	−1.54	−1.79	30	−2.75	−3.26
7	60	0	0.08	10	−0.06	0.21
	50	−0.06	0.18	20	−0.17	0.38
	40	−0.12	0.31	30	−0.23	0.54

The frequency and magnitude shift (relative to dB) in percent from each peak (fault severity) to the healthy is shown.

Subsequently, damage was sequentially introduced at a distance of 50 cm from the clamped end (element 21, see Fig. 1) in three severity levels, a Young's modulus drop from 70 to 60, 50 and 40 GPa. In a similar way the pseudo-fault had three cases where an equivalent mass of 10, 20 and 30 g was added. Table 4 summarises the effect of both stiffness reduction and density increase on the peaks and the troughs of the transmissibility. It shows a comparable behaviour to that found by

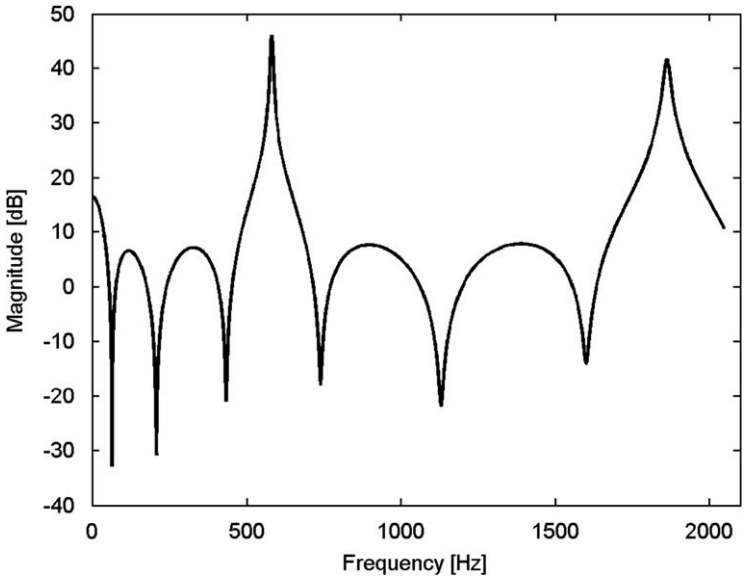

Fig. 5. Healthy transmissibility from FRF ratios calculated from response at 75 cm over that at 25 cm when the excitation was at (75 cm) the free end of the beam.

Table 4
Summary of the effect of stiffness reduction and density increase on the transmissibility peaks and troughs (see Fig. 5).

Peak or trough	Stiffness reduction			Density increase		
	E (GPa)	Frequency shift (Percent)	Magnitude shift (Percent) relative to dB	Added mass (g)	Frequency shift (Percent)	Magnitude shift (Percent) relative to dB
1*	60	−0.78	−7.64	10	−1.56	0.19
	50	−0.78	−5.77	20	−3.12	0.17
	40	−2.34	−9.71	30	−4.69	−1.80
2*	60	−0.48	−0.78	10	−0.96	−0.15
	50	−0.96	−1.53	20	−1.93	−0.63
	40	−1.45	−1.04	30	−2.65	−0.51
3*	60	0	0.15	10	0	0.37
	50	0	0.33	20	0	0.54
	40	0	0.53	30	0	0.52
1	60	0	−0.27	10	−0.09	−0.79
	50	0	−0.66	20	−0.09	−1.52
	40	0	−1.27	30	−0.09	−2.27
4*	60	−0.40	−0.48	10	−1.22	−1.54
	50	−1.01	−1.24	20	−2.30	−3.07
	40	−1.76	−2.31	30	−3.31	−4.79
5*	60	−0.40	−0.30	10	−1.20	−0.93
	50	−0.93	−0.72	20	−2.13	−1.81
	40	−1.64	−1.35	30	−2.92	−2.72
6*	60	−0.03	−0.04	10	−0.09	−0.09
	50	−0.06	−0.08	20	−0.16	−0.09
	40	−0.09	−0.15	30	−0.22	−0.11
2	60	0	−0.39	10	0	−1.12
	50	0	−0.93	20	−0.03	−2.15
	40	0	−1.69	30	−0.03	−3.08

The * denotes a trough.

examining the FRF modes (4th, 6th and 7th in Tables 2 and 3) which shows once more a similar pattern for stiffness reduction and density increase.

This pattern, does not appear to be consistent in the case of the first trough, and the reason for that is mainly the lack of frequency resolution, since the uniform line-spacing (of 0.5 Hz) used here seems inadequate. In fact, when the FRFs were

computed with a resolution of 0.1 Hz for the frequency range of the first trough, the results displayed a monotonic behaviour in the magnitude shifts as well as smaller percentages than those appearing in Table 4. Most importantly there was again a similar pattern in stiffness reduction and density increase. The same reason can be claimed again for any zero frequency shift in Table 4. Both peaks and troughs were considered equivalent as potential features and are numbered consecutively.

Next, features were constructed from the peaks and the troughs of the transmissibility (see Fig. 5). Each feature had a dimension of 20 samples (spectral lines). They were then copied 1000 times and each was corrupted with different white Gaussian noise vectors of a standard deviation of 0.02 for the six troughs and a standard deviation of 2 for the two peaks. This procedure was carried out for the healthy pattern and for each of the three damage cases for both approaches (stiffness reduction–density increase). Features from peaks and troughs are accounted again in a similar way as in Table 4.

The detection algorithm used was outlier analysis described and validated in [12–14]. Basically, a statistical model of the healthy system is created, based on normal data and then subsequent data are tested to see if they are statistically consistent or inconsistent with the normal data. This is actually done by performing a simple statistical test which involves the calculation of a measure called the Mahalanobis squared-distance and then comparing it with a threshold. The threshold depends on the dimension of the problem and it is calculated using a Monte Carlo approach. It can be exclusive or inclusive depending upon whether the sample being tested is included or not in the computation of the statistics for the Mahalanobis distance. In the numerical study, an exclusive threshold was used and since all features have the same dimensions (20×1000), its value is always the same. The value used here corresponds to the 99 percent confidence in identifying an outlier. A detailed description of the threshold calculation can be read in [14] and further reference to outlier analysis may be found in [15].

In the following Figs. 6–13, the Mahalanobis squared-distance for all the extracted features is plotted. The horizontal dashed line represents the exclusive threshold. It is clear that some features such as the one from the 3rd and 6th trough of the transmissibility proved to be not sensitive to damage. In order to assess the relative sensitivity of each of the eight features to mass addition and stiffness reduction, the mean Mahalanobis distance values across each set of 1000 observations, normalised by the threshold, are calculated. In Table 5, these values are shown for the eight features (six troughs and two peaks). In Table 6 the features are ranked according to the normalised Mahalanobis distances when they were averaged for all severity cases: the feature ranked '1st' is the most sensitive to 'damage' for the given state, and the feature ranked '8th' the least sensitive.

By looking at all data from the numerical simulation some brief conclusions can be made. Although the location of the fault significantly changes its effect on the structure, a similar pattern was observed in the comparison of the two ways of simulating it (stiffness or density) as seen in Figs. 3 and 4 as well as in Tables 2–4. In addition, in Table 6 the ranking of the features when all the severity cases were averaged is shown. A careful look shows an exact match in the feature ranking for 6 out of the 8 features, and that always includes the best and the worst feature. If the same principle is followed for the ranking of the features for each damage case (from Table 5), then the same match (6 out of 8) will be found again.

The discrepancy in the feature ranking is found in the first trough and the first peak, so it could be reasonable to think that it may be caused by the lack of resolution (as described earlier) or by excessive added noise. The calculation of the transmissibility function with a finer resolution of 0.1 improved the magnitude shifts (Table 4) for the first trough, but since the feature ranking was in a satisfactory agreement for all cases, the repetition of the whole novelty detection procedure was deemed unnecessary. Another reason for the above ranking disagreement might be also the damage location.

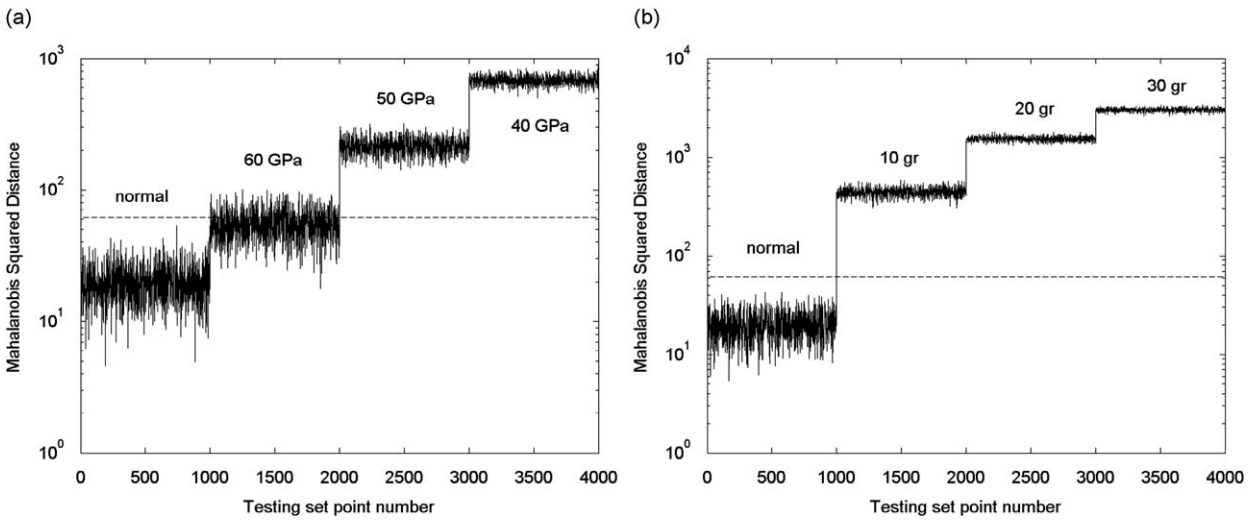

Fig. 6. Outlier statistics for stiffness reduction (a) and density increase (b), feature created from the first trough of the transmissibility function taken at 75 cm over 25 cm of the beam.

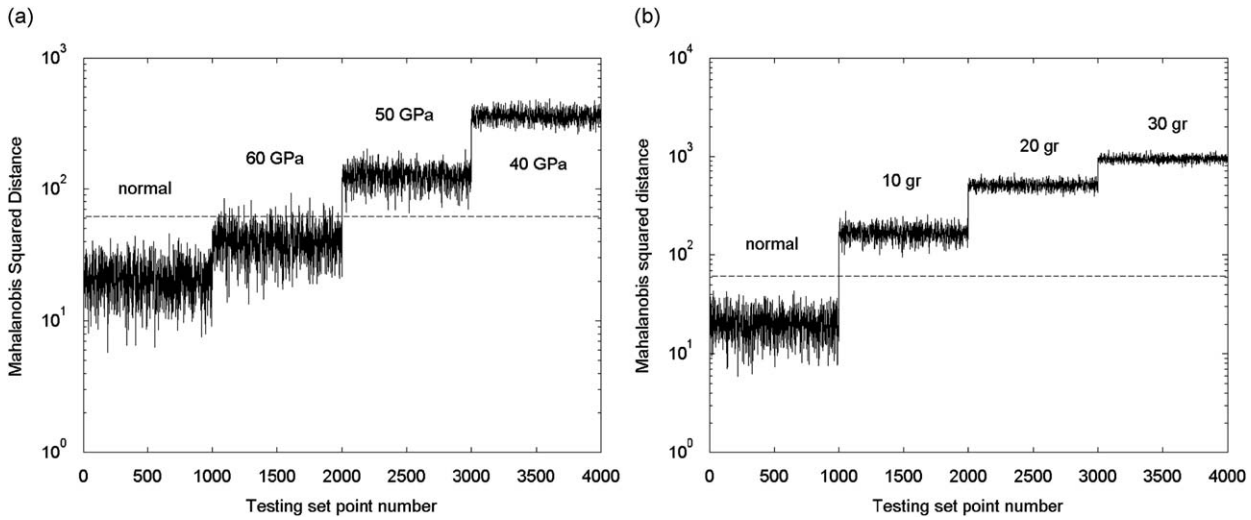

Fig. 7. Outlier statistics for stiffness reduction (a) and density increase (b), feature created from the second trough of the transmissibility function taken at 75 cm over 25 cm of the beam.

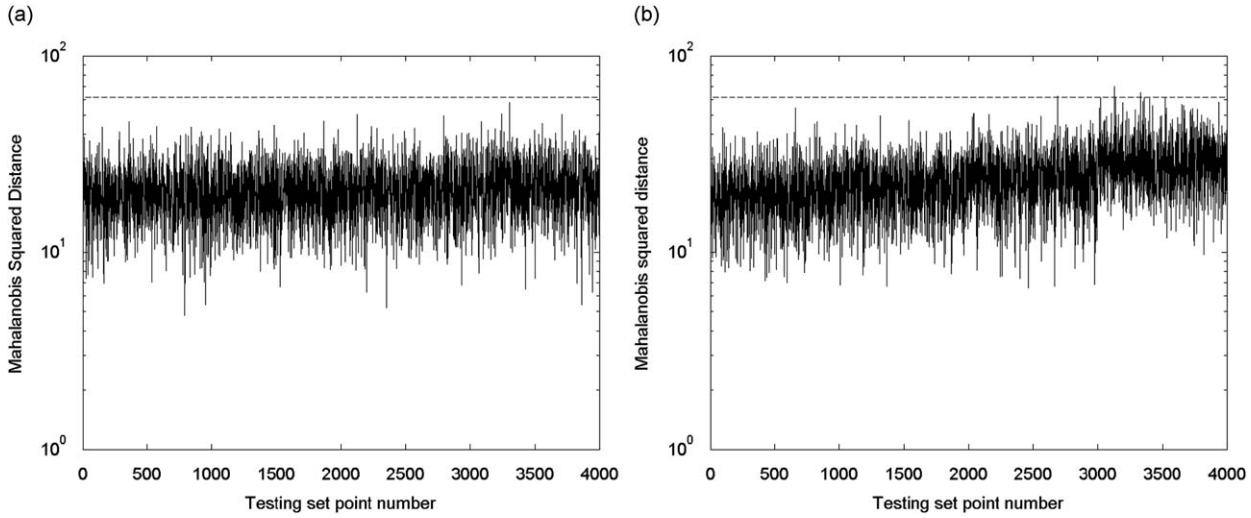

Fig. 8. Outlier statistics for stiffness reduction (a) and density increase (b), feature created from the third trough of the transmissibility function taken at 75 cm over 25 cm of the beam.

The latter is valid on this specific structure since an added mass on a cantilever beam has a stronger effect towards the free edge while a change in the stiffness has a stronger effect towards the clamped end. The important point here is that the features which lead to insensitive novelty detectors are unambiguously detected.

4. Test setup and data acquisition for the experimental part of the study

The experimental part of the study was a logical step after the promising results of the FE simulation. The structure under consideration was a stiffened aluminium panel intended to replicate an aircraft wingbox. The top sheet of the wingbox is a $750 \times 500 \times 3$ mm aluminium sheet. This is stiffened by the addition of two ribs composed of lengths of C-channel riveted to the shorter edges and two stiffening stringers composed of angle section that are bolted along the length of the sheet as shown in Fig. 14. Free–free boundary conditions are approximated experimentally by suspending the wingbox from a substantial frame using springs and nylon line attached at the corners of the top sheet.

In order to validate the whole added mass approach, a real damage scenario was introduced in the form of a saw-cut. The location of the fault, in all cases, was at the outside stringer 125 mm from the edge of the panel (Figs. 14 and 15). Four severity levels were investigated for both scenarios. So, a sequential increase of the added mass from 25 g to 50, 75 and

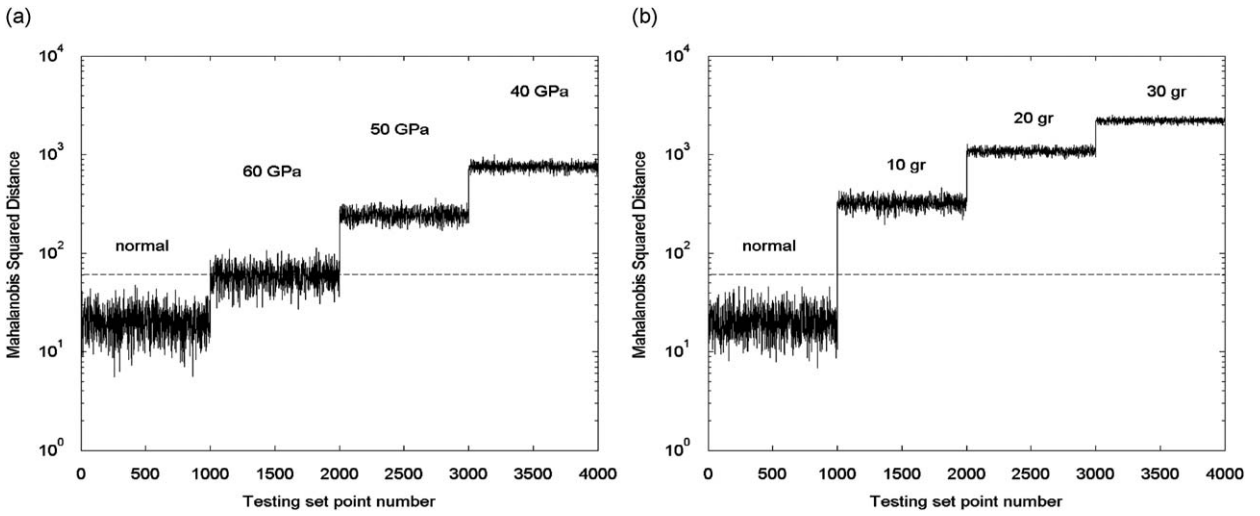

Fig. 9. Outlier statistics for stiffness reduction (a) and density increase (b), feature created from the first peak of the transmissibility function taken at 75 cm over 25 cm of the beam.

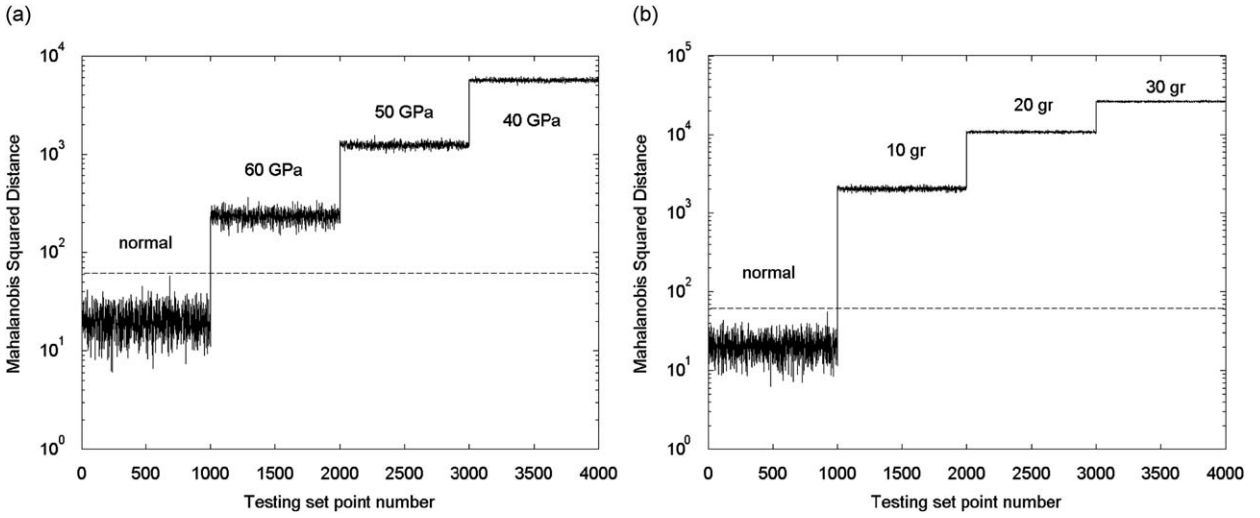

Fig. 10. Outlier statistics for stiffness reduction (a) and density increase (b), feature created from the fourth trough of the transmissibility function taken at 75 cm over 25 cm of the beam.

100 g (Fig. 15) was followed by a 25, 50, 75 and 100 percent saw-cut on the stringer. These cuts correspond to depths of 5.5, 11, 16.5 and 22.5 mm. The overall mass increase in percentage form is 0.42 to 0.84, 1.25 and 1.67 percent.

The acquisition system used during the test was a DIFA SCADAS III controlled by LMS software running on a Dell desktop PC. All measurements were recorded within a frequency range of 0–1600 Hz with a resolution of 0.5 Hz. The 'wingbox' was excited with a white Gaussian signal through an LDS shaker powered by an amplifier of the same brand and the responses were measured using unidirectional PCB piezoelectric accelerometers attached vertically at the locations shown in Fig. 14. The excitation was measured using a standard force transducer. The base measurements were FRFs, acquired using sensors 1 and 2 (Fig. 14) which were next used to form transmissibility functions. Only the magnitudes of the measurements were used in this study, the phase was discarded. These raw data were then employed in the construction of novelty detectors in a similar scheme as that in Refs. [12,13]. The whole process was equivalent to that of the numerical study since outlier analysis was again the main tool to create the novelty detectors, but this time all data originated from experiment.

The test order for the programme and configuration was as follows:

1. Normal condition;
2. 25 g mass added;
3. 50 g mass added;

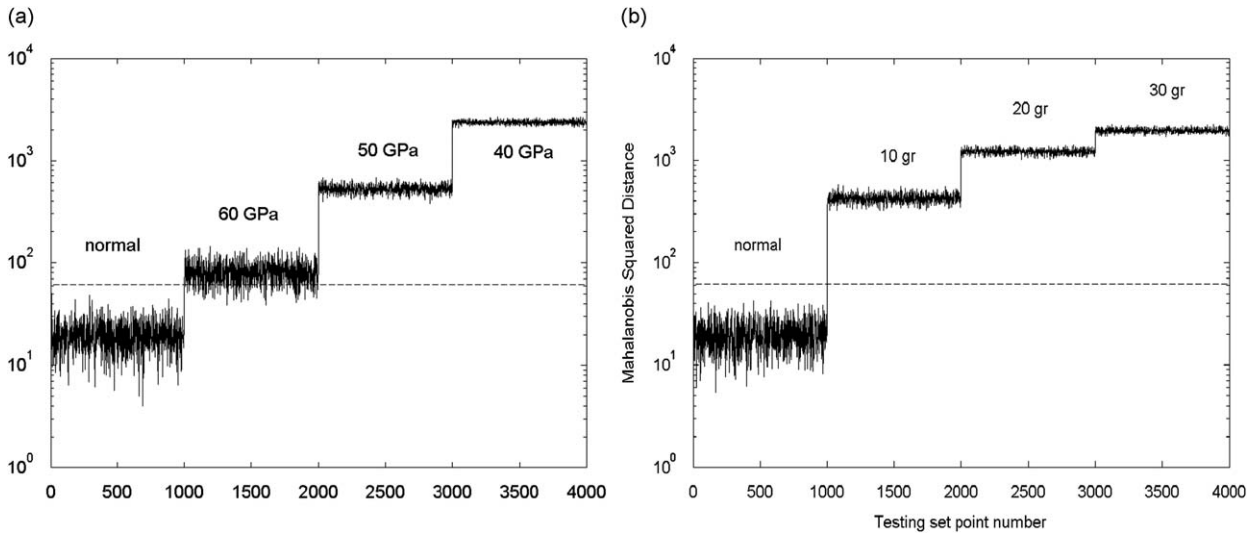

Fig. 11. Outlier statistics for stiffness reduction (a) and density increase (b), feature created from the fifth trough of the transmissibility function taken at 75 cm over 25 cm of the beam.

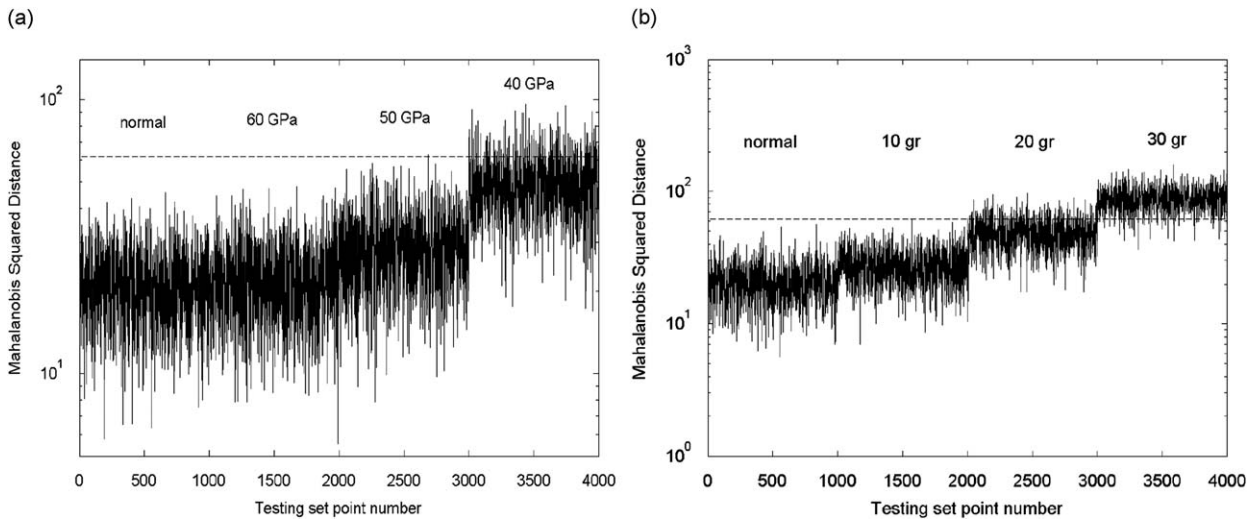

Fig. 12. Outlier statistics for stiffness reduction (a) and density increase (b), feature created from the sixth trough of the transmissibility function taken at 75 cm over 25 cm of the beam.

4. 75 g mass added;
5. 100 g mass added;
6. normal condition;
7. 25 percent saw-cut on the stringer;
8. 50 percent saw-cut on the stringer;
9. 75 percent saw-cut on the stringer; and
10. 100 percent saw-cut on the stringer.

Overall this meant that two sets of measurements for normal condition were acquired and one for each of the four severity cases for both forms of 'damage'. Each configuration (set) consisted of a signal acquired with 40 averages, to be used as a 'clean' reference for the feature selection later and then 100 measurements taken sequentially using only two averages. The two normal condition settings had each 200 of the same two-average 'shots'. The low-average signals formed the multivariate features which were used to create novelty detectors with outlier analysis.

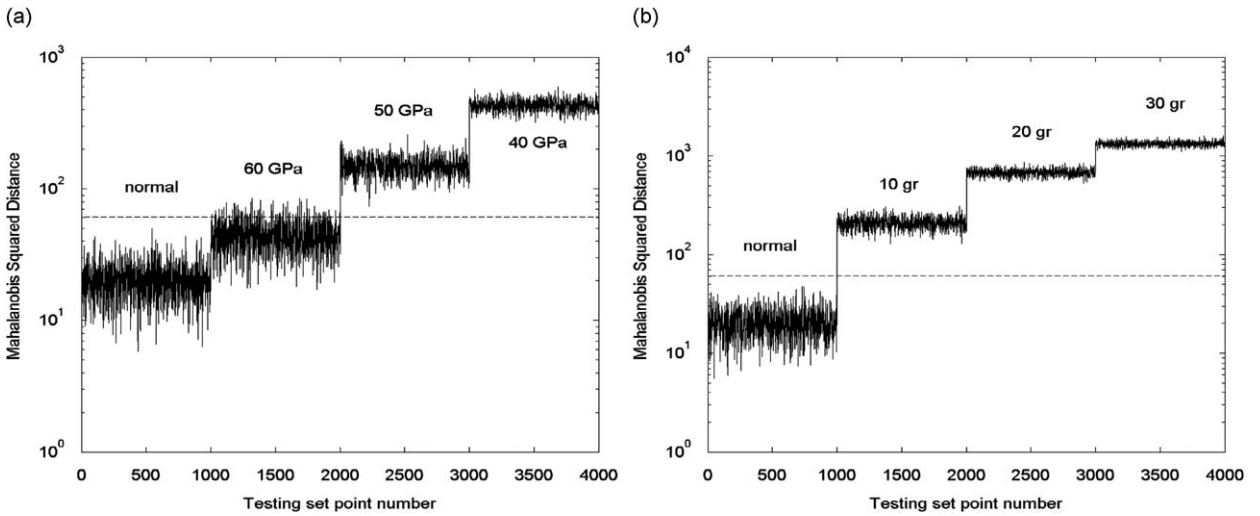

Fig. 13. Outlier statistics for stiffness reduction (a) and density increase (b), feature created from the second peak of the transmissibility function taken at 75 cm over 25 cm of the beam.

Table 5
Normalised Mahalanobis squared distance for stiffness reduction and density increase for all the damage severity cases.

Peak or trough	Stiffness reduction			Density increase		
	60 GPa	50 GPa	40 GPa	10 g	20 g	30 g
1*	0.90	3.54	11.12	7.15	24.86	49.14
2*	0.66	2.07	5.91	2.71	8.24	15.42
3*	0.33	0.34	0.37	0.36	0.40	0.48
1	0.99	4.00	12.38	5.30	17.66	36.14
4*	3.80	20.25	91.90	32.91	175.38	428.24
5*	1.31	8.53	38.68	14.10	70.64	162.15
6*	0.34	0.40	0.54	0.45	0.79	1.44
2	0.73	2.44	7.05	3.41	11.05	21.70

The * denotes a trough.

Table 6
Normalised Mahalanobis distance averaged for all severity cases along with the ranking of the eight features for stiffness reduction and density increase.

Peak or trough	Average severity Mahalanobis distance over threshold/ranking			
	Stiffness reduction		Density increase	
1*	5.18	4th	27.05	3rd
2*	2.88	6th	8.79	6th
3*	0.35	8th	0.41	8th
1	5.79	3rd	19.70	4th
4*	38.65	1st	212.18	1st
5*	16.18	2nd	82.30	2nd
6*	0.42	7th	0.89	7th
2	3.40	5th	12.05	5th

The * denotes a trough.

5. Feature selection and novelty detection for the experimental part of the study

This could be arguably called one of the most important stages in a structural health monitoring project. In this experimental part of the study a feature is a region of the given transmissibility which separates unambiguously the

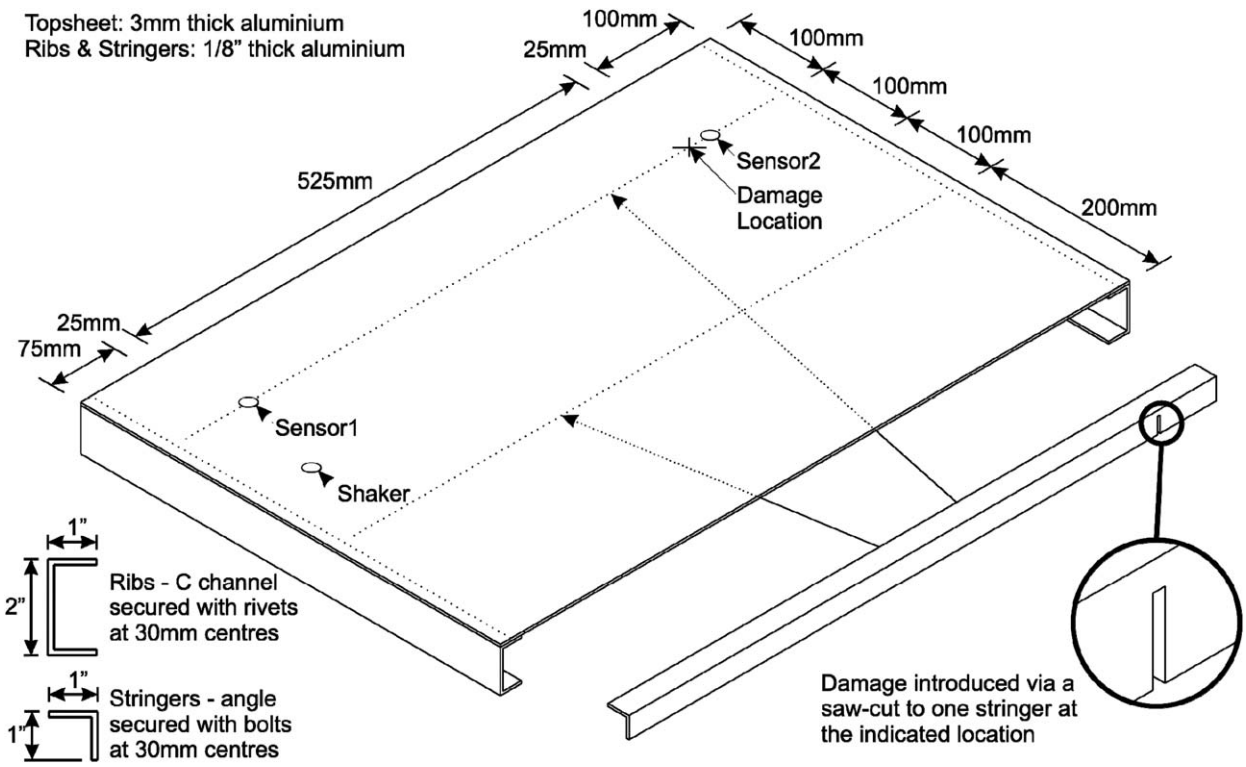

Fig. 14. Schematic of the experimental structure.

Fig. 15. Photograph of the 'aircraft wingbox' with mass added on one of its stringers.

normal condition data from the damage data. In previous work [13], potential features were judged as strong, fair or weak according to the following criteria:

- A *strong* feature is a region of the frequency range on which the normal data and damage data appear to be structurally different. Also, the damage data should be strongly separated compared to the spread of the normal data.
- A *fair* feature is a region of the frequency range on which the normal data and damage data appear to be structurally different *or* the damage data are strongly separated compared to the spread of the normal data.
- A *weak* feature is a region of the frequency range on which the normal data and damage data are separated.

Following those guidelines the next step was an extensive visual search through the measured data for potential features that could form novelty detectors. This process gave a significant number of fair, strong and weak features.

The final selection was done on the logarithmic magnitude values of the measurements and it was based on the ranking of their performance as novelty detectors. That was again the ratio of the Mahalanobis distance over the threshold, as done before for the case of the cantilever beam.

As a first approach, all the feature selection was carried-out based on all four severity cases for the added masses (i.e. the pseudo-damage) at the same time. Although, this might lead to insensitive novelty detectors for some of the severity cases, it can make the comparison with the saw-cut scenario more convenient. Consequently, the final selection was determined by ranking the average value of the features. Figs. 16–21 show the performance of the final 6 selected features on the added mass and on the saw-cut data. Their number was chosen arbitrarily, but was enough to make the study comparable to that of the numerical simulation.

By examining the above figures some interesting facts can be revealed. All the features seem to work adequately on the mass and on the saw-cut data as well, except the last one (Fig. 21), which does not perform so well for the 25 and 50 percent saw-cut. In addition, features 1, 2, 4 and 6 (Figs. 16, 17, 19 and 21) show a monotonic increase in the Mahalanobis distance as the size of the mass increases. This behaviour is expected, as the addition of larger masses should lead to a greater discordancy value. However, this is not happening in features 3 and 5 (Figs. 18 and 20). The reason for that is primarily the fact that the features were selected by examining all severity cases at the same time and based on their average ranking. This means that in the effort to select a 'general' feature that would always work, significant regions might have been left out in some of the four severity cases. These regions could mark a feature as strong, fair or weak, according to

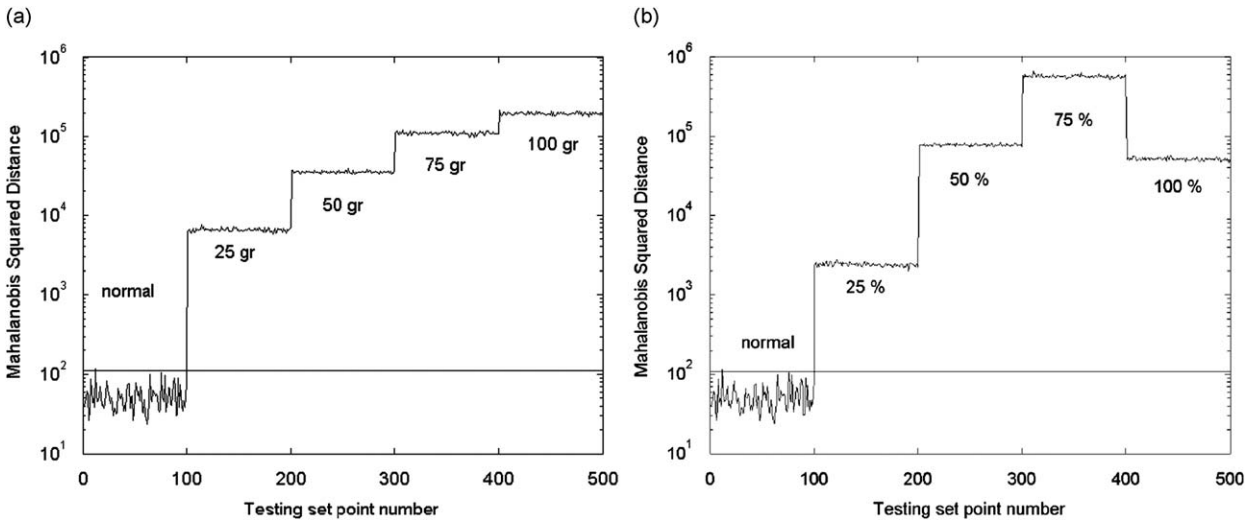

Fig. 16. Outlier statistics for the highest (average) ranking feature on the added mass (a) and on the saw-cut data (b).

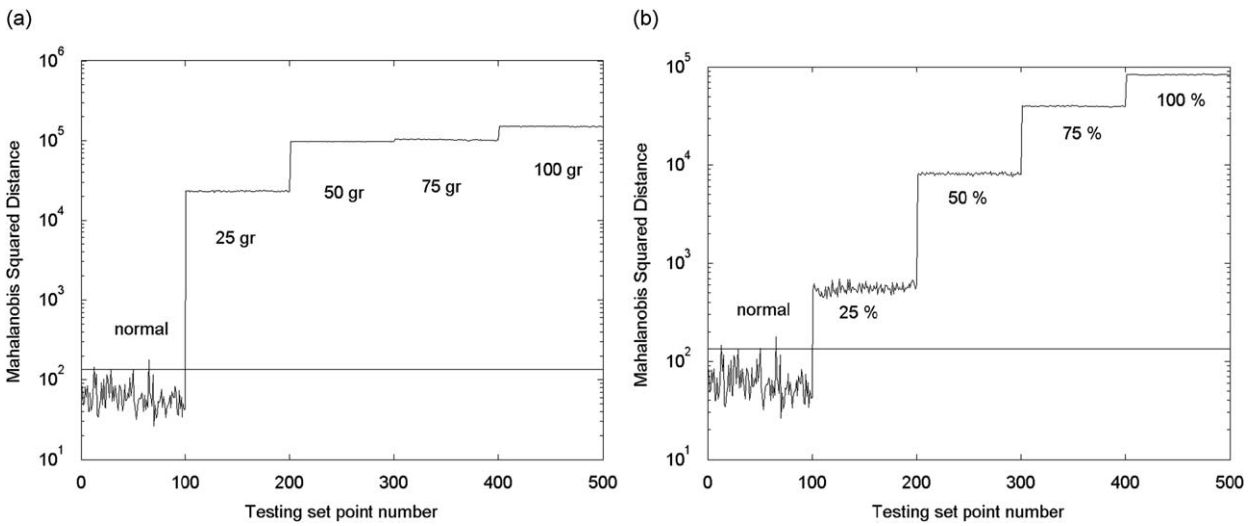

Fig. 17. Outlier statistics for the second (average) ranking feature on the added mass (a) and on the saw-cut data (b).

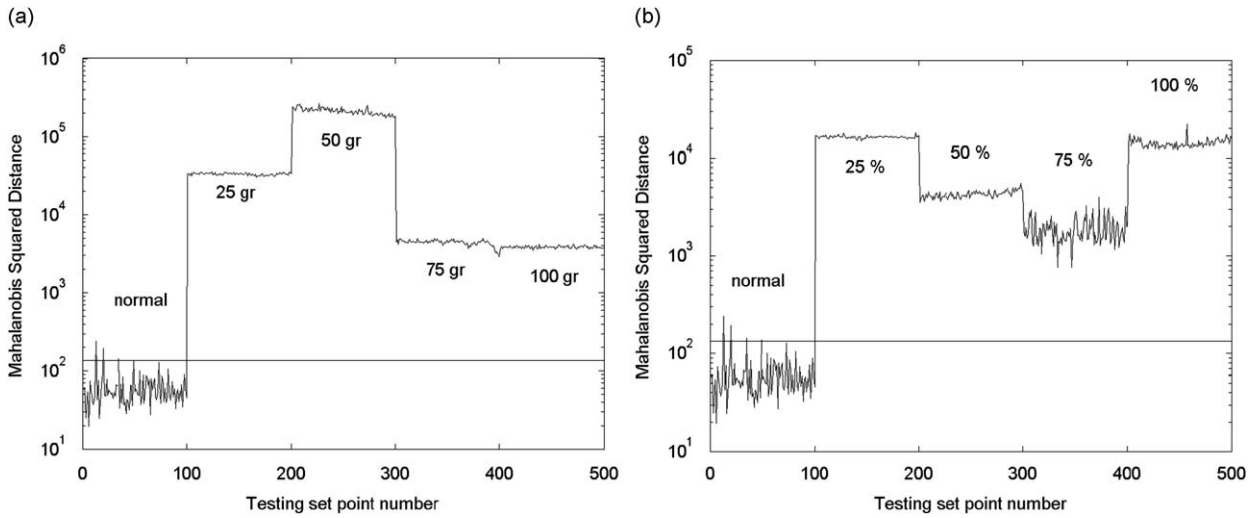

Fig. 18. Outlier statistics for the third (average) ranking feature on the added mass (a) and on the saw-cut data (b).

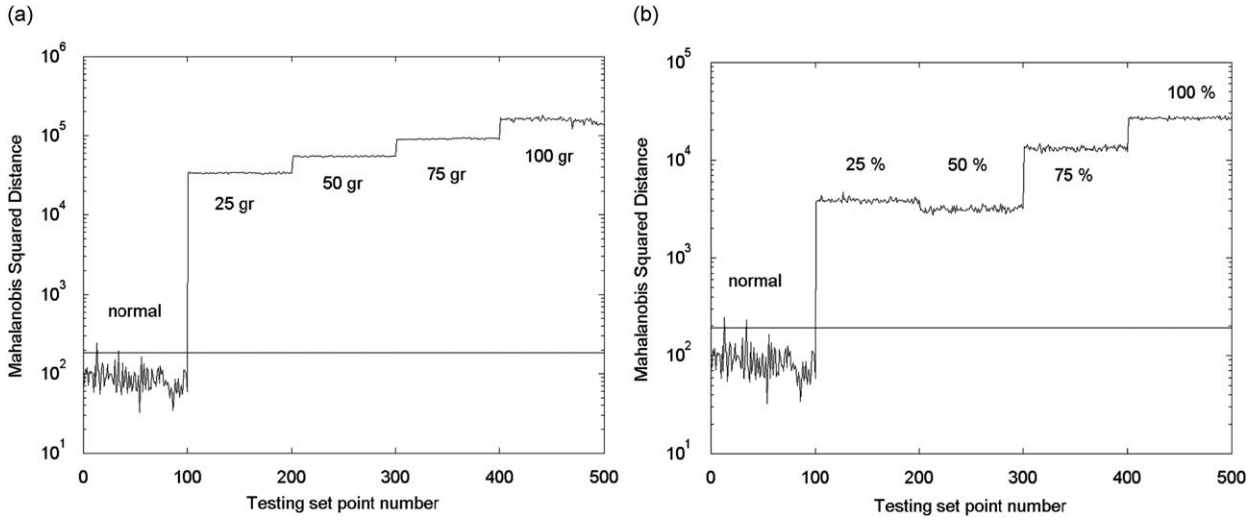

Fig. 19. Outlier statistics for the fourth (average) ranking feature on the added mass (a) and on the saw-cut data (b).

the criteria used in the study. It is reasonable to say that this is more evident in the largest mass case since its effect on the transmissibility functions is also stronger.

The same reason can be easily claimed for the poor performance of the two lowest severity cases on the 6th feature (Fig. 21). This can actually be shown by examining the data for that feature (Fig. 22) where it is clear that it is not ideal for the lowest added mass case since there is significant overlap with the normal data. The same figure also reveals an adjacent transmissibility region that appears to be more suited for the 25 g case. The importance of this selection is clearly displayed on Fig. 23 where the feature's performance on the added mass and the saw-cut data is shown to be satisfactory.

It should be noted, however, that inspection of all the data reveals multiple features which also perform adequately for the 25 g case and selecting features based only on that case would lead to the same five features as before (based on all cases) and an additional 6th one, which still performs well on the saw-cut data. The important point here is that by choosing features based only on the lowest added mass case it is still feasible to construct novelty detectors that perform well on real damage. This can be considered a critical part of this work.

In Table 7 the ranking of the six selected features is displayed. There is an agreement on the first and on the worst, but not in the features between. This is not considered crucial here, since the object of this work was not to cause exactly the same change in the system (added mass—saw-cut), but rather to find the strategy needed to select features that will lead to novelty detectors capable of being used by a PR algorithm.

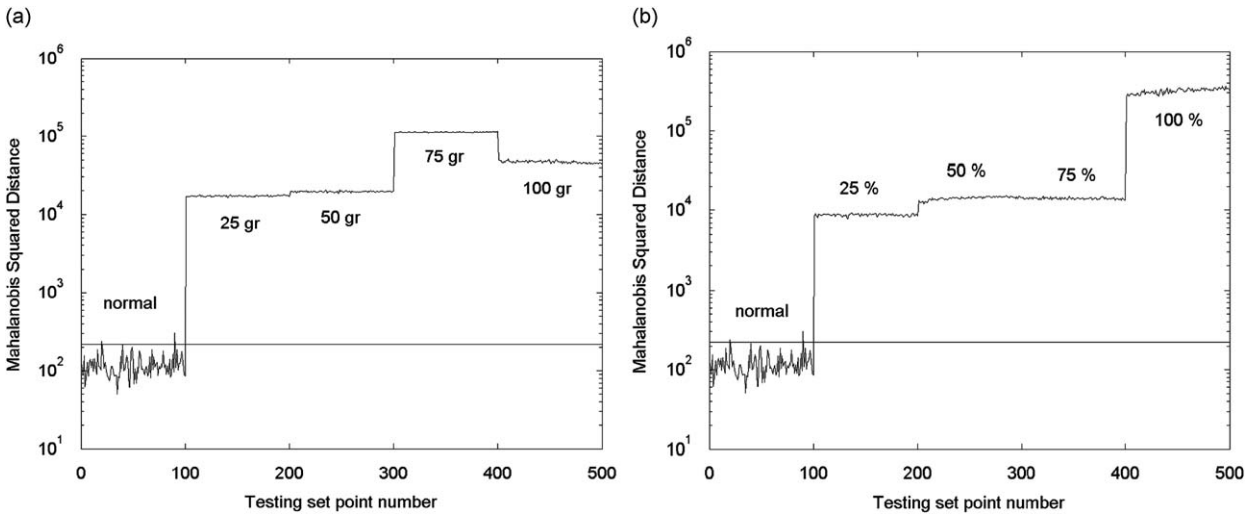

Fig. 20. Outlier statistics for the fifth (average) ranking feature on the added mass (a) and on the saw-cut data (b).

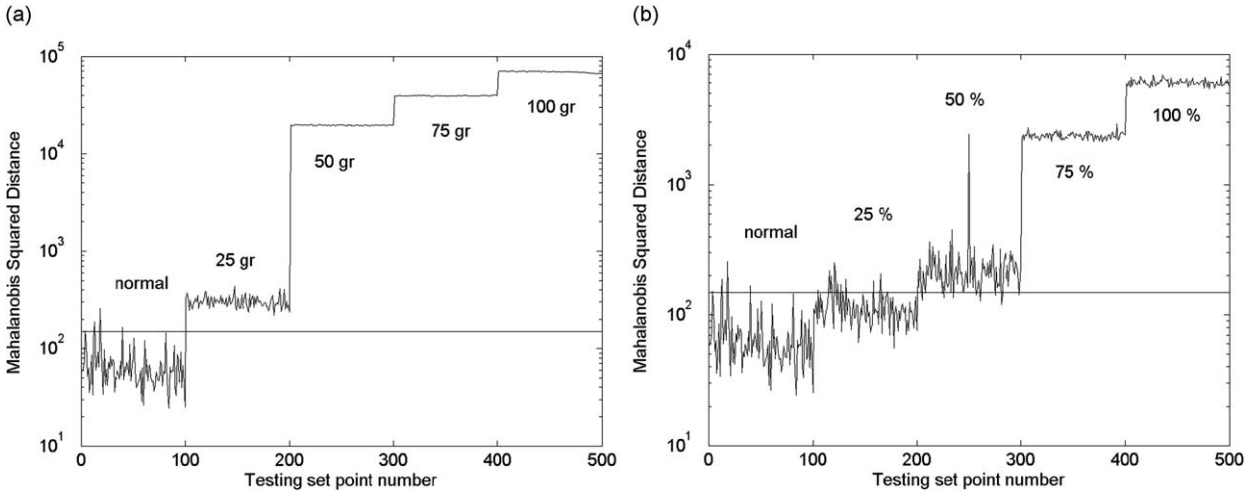

Fig. 21. Outlier statistics for the last (average) ranking feature, of the 6 selected, on the added mass (a) and on the saw-cut data (b).

Clearly, just the fact that the worst and the best are equally identified can be judged as sufficient and it could mark as successful the transition from the simple FE beam model, to a more complex laboratory structure. Nonetheless, it should be noted that choosing the features which also show a monotonic increase in the discordancy value with the increase of the severity state, from the six ones with the highest average ranking (Mahalanobis distance over threshold) leads to a final selection of four (the 1st, 2nd ,4th and 6th). Those features work again for both cases, except the same last one as before and their ranking is exactly matched, as seen in Table 8.

5. Discussion and conclusions

The object of this work was to explore the possibility of applying a simple and non-destructive way of inducing pseudo-faults in a structure for the purpose of damage identification and ultimately to define the experimental strategy to do so. The main idea is that by adding masses on a structure, an effect can be potentially observed on the system, similar to that a reduction in stiffness would cause. The feature selection in that case can lead to damage indicators and this in turn will allow the availability of training data for any pattern recognition (PR) algorithm.

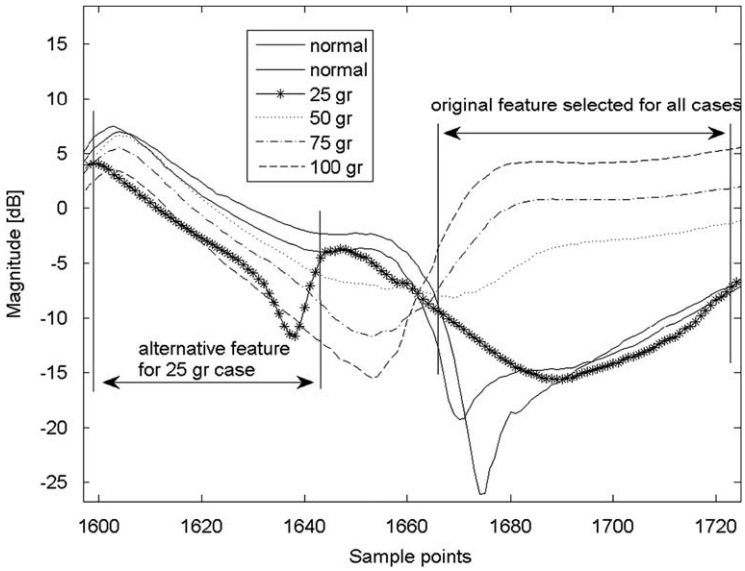

Fig. 22. Original feature 6 (in transmissibility function) and the adjacent one that works for the lowest severity case.

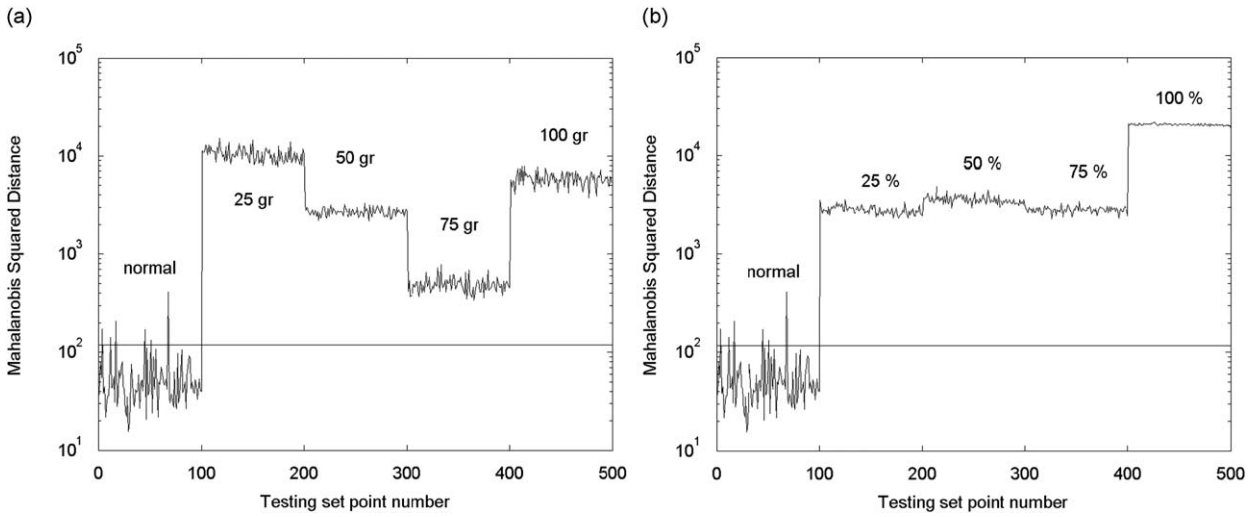

Fig. 23. Outlier statistics for the adjacent feature from Fig. 22 (selection based on 25 g case) on the added mass data (a) and on the saw-cut data (b).

Table 7
Ranking of the six selected features for both the added mass and the saw-cut cases.

Ranking for added mass	Average Mahalanobis distance over threshold	Ranking for saw-cut	Average Mahalanobis distance over threshold
1st	806.75	1st	1598.00
2nd	675.11	3rd	243.06
3rd	466.76	4th	68.96
4th	456.57	5th	60.85
5th	222.95	2nd	395.19
6th	215.23	6th	14.66

To demonstrate this, a simple cantilever beam was first simulated with FE analysis. Damage was introduced in the form of a reduction of the Young's modulus on one of the elements and the pseudo-fault was modelled with an increase in its density. This first part of the work mainly showed the existence of similar patterns in both cases (stiffness loss and density increase) despite the influence of the location of the fault. In addition, it was feasible to create features that would lead to

Table 8
Ranking of the four selected features (out of the original 6) which show a monotonic increase in the Mahalanobis distance with the increase of the damage magnitude.

Ranking for added mass	Average Mahalanobis distance over threshold	Ranking for saw-cut	Average Mahalanobis distance over threshold
1st	806.75	1st	1598.00
2nd	675.11	2nd	243.06
3rd	456.57	3rd	60.85
4th	215.23	4th	14.66

novelty detectors from both cases of damage simulation. When those features were ranked, according to the ratio of the Mahalanobis distance over the threshold, it was found that there was a satisfactory agreement on all severity cases tested with the best and the worst feature equally identified.

The next logical step was the application of the method on a real laboratory structure, an aluminium aircraft wingbox. An actual saw-cut was made to work as a benchmark for the pseudo-fault. Four different severity cases were used for both scenarios. Features were selected and novelty detectors were constructed from both the added mass and the saw-cut data. The most essential and also promising part of this work was that those features performed well on both cases. There was of course an exception to the last one, the worst based on their ranking, but it could be amended when the features are selected based on the lowest severity case. The feature ranking was not identical, except from the case when there was a final selection of only four features which showed a monotonic increase on the Mahalanobis distance with the increase of the 'damage' magnitude. However, the best and the worst were again always exactly matched.

Nevertheless, since the object here was not to prove that both scenarios are identical, this can lead to a positive claim that there exists a relation between an added mass and structural damage which can be used in a PR methodology. In the same spirit, the size of the mass needs only to be enough to cause changes to the system, unless a damage severity task is attempted. At this stage of research it cannot be claimed that using this pseudo-fault approach is something generic. In a more complicated structure, such as an aircraft wing, more challenges are likely to be encountered. The effect of a mass on such a system will have an inverse behaviour to that of a saw-cut while its location moves along its length. Features which can still work on both scenarios (mass—saw-cut) might present enough structural differences to make a PR algorithm struggle.

However, it can be said with more confidence that it is feasible to construct novelty detectors without actually damaging a structure. As networks of novelty detectors have proved capable of locating and sizing damage in previous works; the proposed method of generating training data may also offer a reasonable prospect of progressing up the levels in the damage detection hierarchy. In fact, in the restricted situation where damage location can be cast as a classification problem (i.e. damage is at site A *or* damage is at site B *or*…), the pseudo-fault strategy has already proved itself capable of generating training data in a quite demanding experimental situation, and this will be reported in detail elsewhere.

The strategy of adding masses is not offered here as a panacea and the authors are convinced that there will be situations where it does not provide the appropriate information. However, it is in the authors' belief that the strategy may provide one of the tools in a 'toolbox' which may prove capable of extending the use of pattern recognition methods beyond their current limits. As a further stimulus to research, one might add that there may well be other pseudo-faults, not added masses, which prove capable of attacking other types of problem. The authors believe that there is considerable merit in the application of machine learning to SHM problems and further believe that the problem of the origin of training data can be solved in practical and affordable terms; it is this belief which is currently the subject of further investigations.

References

[1] J.E. Doherty, Nondestructive evaluation, in: A.S. Kobayashi (Ed.), *Handbook on Experimental Mechanics*, Society for Experimental Mechanics, Inc., 1987 (Chapter 12).
[2] S.W. Doebling, C.R. Farrar, M.B. Prime, A summary review of vibration-based damage identification methods, *The Shock and Vibration Digest* 30 (1998) 91–105.
[3] A. Rytter, Vibration-Based Inspection of Civil Engineering Structures, Ph.D. Thesis, University of Aalborg, Department of Building Technology and Structural Engineering, 1993.
[4] H.M. Kim, T.J. Bartkowicz, An experimental study for damage detection using a hexagonal truss, *Computers and Structures* 79 (2) (2001) 173–182.
[5] S. Sundararaman, D.E. Adams, E.J. Rigas, Structural damage identification in homogeneous and heterogeneous structures using beamforming, *Structural Health Monitoring* 4 (2) (2005) 171–190.
[6] C.H. Wang, J.T. Rose, F.K. Chang, A synthetic time-reversal imaging method for structural health monitoring, *Smart Materials and Structures* 79 (2) (2001) 173–182.
[7] P.J. Fanning, E.P. Carden, Experimentally validated added mass identification algorithm based on frequency response functions, *Journal of Engineering Mechanics* 130 (9) (2004) 1045–1051.
[8] W. Ostachowicz, M. Krawczuk, M. Cartmell, The location of a concentrated mass on rectangular plates from measurements of natural vibrations, *Computers and Structures* 80 (16–17) (2002) 1419–1428.
[9] L.Y. Cheung, K. Worden, J.A. Rongong, Damage detection in an aircraft component mode, *Proceedings of the 19th International Modal Analysis Conference, IMAC*, Vol. XIX, Kissimmee, Florida, February 2001, pp. 1234–1241.

[10] M. Weiland, M. Link, *Matfem 99 User's Guide*, *Version 26-May-2000*, University of Kassel, 2000.
[11] R. Blevins, *Formulas for Natural Frequency and Mode Shape*, Krieger Publishing Company, 1984.
[12] G. Manson, K. Worden, D.J. Allman, Experimental validation of a structural health monitoring methodology: part II. Novelty detection on a gnat aircraft, *Journal of Sound and Vibration* 259 (2) (2003) 345–363.
[13] G. Manson, K. Worden, D.J. Allman, Experimental validation of a structural health monitoring methodology: part III. Damage location on an aircraft wing, *Journal of Sound and Vibration* 259 (2) (2003) 365–385.
[14] K. Worden, G. Manson, N.R.J. Fieller, Damage detection using outlier analysis, *Journal of Sound and Vibration* 229 (3) (2000) 647–667.
[15] V. Barnett, T. Lewis, *Outliers in Statistical Data*, Wiley, Chichester, 1994.